tvst

Retina

Dome-Shaped Macula Curvature: A New Quantitative Metric to Assess Dome-Shaped Macula Subtypes

Sebastiano Del Fabbro[1,2], Alessandro Arrigo[1–3], Lorenzo Bianco[1,2], Alessio Antropoli[1,2], Annamaria Nunziata[1,2], Ugo Introini[1,2], Daniele Giusto[4], Francesco Bandello[1,2], and Maurizio Battaglia Parodi[1,2]

[1] School of Medicine, Vita-Salute San Raffaele University, Milan, Italy
[2] Ophthalmology Unit, IRCCS San Raffaele Scientific Institute, Milan, Italy
[3] Eye Repair Unit, Division of Neuroscience, IRCCS San Raffaele Scientific Institute, Milan, Italy
[4] Department of Electrical and Electronic Engineering, University of Cagliari, Cagliari, Italy

Correspondence: Alessandro Arrigo, Ophthalmology Unit, IRCCS San Raffaele Scientific Institute, Via Olgettina, 60, Milan, Lombardy 20132, Italy. e-mail: alessandro.arrigo@hotmail.com

Received: January 10, 2025
Accepted: June 3, 2025
Published: August 4, 2025

Keywords: dome-shaped macula; dome-shaped macula curvature; optical coherence tomography; high myopia; choroidal thickness

Citation: Del Fabbro S, Arrigo A, Bianco L, Antropoli A, Nunziata A, Introini U, Giusto D, Bandello F, Battaglia Parodi M. Dome-shaped macula curvature: A new quantitative metric to assess dome-shaped macula subtypes. Transl Vis Sci Technol. 2025;14(8):9, https://doi.org/10.1167/tvst.14.8.9

Purpose: To test a new quantitative metric focused on the evaluation of dome-shaped macula curvature (DSMC); to assess its clinical role in evaluating round (R-DSM), vertical (V-DSM), and horizontal (H-DSM) DSM types; and to examine its relationships with other ocular parameters.

Methods: Patients affected by DSM secondary to high myopia were included in this cross-sectional, observational case study. DSMC was calculated by measuring the base (chord length) and height (distance from the chord to the apex) of the DSM. These measurements were used to determine the radius (R) of the hypothetical circle representing the curvature of the DSM. Curvature (K) was then calculated as the reciprocal of R. In addition, we measured choroidal thickness (CT), best-corrected visual acuity (BCVA), and spherical equivalent (SE) to assess its potential relationship with DSMC.

Results: A total of 125 eyes from 107 patients (25 males, 23%) were included, with a mean age of 65.67 $\pm$ 13.51 years. DSM subtypes—categorized as 57 R-DSM eyes (45.6%), 58 H-DSM eyes (46.4%), and 10 V-DSM eyes (8%)—showed significantly different DSMC ($P = 0.039$), with R-DSM showing the highest DSMC values. Conversely, V-DSM and H-DSM were characterized by similar DSMC. Subfoveal CT showed a strong inverse correlation with DSMC ($P < 0.0001$; $r = -0.60$), with a consistent reduction in CT as curvature increased. DSMC was also significantly associated with SE, with higher DSMC values corresponding to greater myopic refractive errors ($P = 0.009$; $r = -0.21$).

Conclusions: DSMC may be considered a reliable and reproducible quantitative metric to analyze DSM subtypes. The association of DSMC with CT highlights the influence of scleral curvature on choroidal morphology and trophism, paving the way for future new outcome measures.

Translational Relevance: DSMC provides an objective and reproducible method to evaluate DSM morphology across subtypes (round, vertical, and horizontal). By quantifying curvature through OCT-based parameters, this metric enables standardized comparisons and enhances the clinical characterization of DSM. Furthermore, the study provides insights into the disease mechanisms by uncovering significant associations between DSMC and choroidal thickness.

Introduction

A dome-shaped macula (DSM) is defined as a convex, curved, and elevated macular profile within the concavity of the staphyloma,[1] commonly observed in high myopia. Although its pathogenesis remains unclear, it has been associated with localized scleral thickening.[2,3] Its occurrence varies with ethnicity,[1,4] with the greatest prevalence in Asian populations, corresponding to at least 20% of cases[5]; however, it is also described in hyperopic, emmetropic, and moder-

Copyright 2025 The Authors

This work is licensed under a Creative Commons Attribution-NonCommercial-NoDerivatives 4.0 International License.

ately myopic eyes.[6,7] DSM has been associated with several complications, including serous retinal detachment (SRD), choroidal neovascularization (CNV), and vitreomacular interface disorders.[1,5,8,9]

The current DSM categorization is based on the assessment of its morphology by multimodal retinal imaging. Two distinct DSM subtypes have been described: dome-shaped and band-shaped, with the latter being significantly more prevalent (82.4%).[10] The band-shaped DSM has been further refined into a ridge-shaped macula (RSM), characterized by macular elevation occurring along only one foveal meridian.[11] RSM may exhibit vertical,[10–12] horizontal,[10–12] or oblique[13] orientations. Despite these categorizations, DSM assessment remains challenging due to the lack of objective, standardized, and reproducible measurement methods.

The present study aimed to develop a quantitative assessment of DSM subtypes based on the measure of DSM curvature (DSMC), in a cohort of patients not affected by complications such as CNV and SRD. Furthermore, the study investigated the associations between DSMC and ocular parameters, including choroidal thickness (CT), spherical equivalent (SE), and best-corrected visual acuity (BCVA).

Methods

Study Design

The study was designed as a cross-sectional, observational case series that included myopic eyes with confirmed presence of DSM on optical coherence tomography (OCT) images (SPECTRALIS HRA2+ OCT; Heidelberg Engineering, Heidelberg, Germany). All of the patients were recruited by retrospectively assessing data records at the ophthalmology unit of IRCCS San Raffaele Scientific Institute, Milan, Italy. The patients signed informed consents before being included in the study. The entire investigation received local ethical approval (MIRD2020), respecting the tenets of the Declaration of Helsinki.

Inclusion criteria included age > 18 years old; high myopia, defined as SE > −6.00 diopters (D)[14]; and the presence of a DSM. The criteria used to define and classify DSM are described in detail in the following text. Exclusion criteria were high media opacity; the presence of subretinal fluid with or without CNV as assessed by OCT and fluorescein angiography examination; stage 4 myopic atrophy as defined by the Meta-Analysis for Pathologic Myopia (META-PM) classification system[15]; any ophthalmic surgery performed within 6 months from the baseline evaluation; any other ocular disorder that might affect data interpretation, including vascular occlusive diseases, uveitis, and optic nerve disorders; poor image quality (Heidelberg HEYEX quality score < 25); previous history of myopia-related complications (e.g., retinoschisis, retinal detachment, vitreoretinal disorders)[16,17]; or any other uncontrolled systemic disorder that might affect data interpretation.

Each patient underwent a complete ophthalmologic examination, including BCVA, slit-lamp biomicroscopy, and spectral-domain OCT. BCVA was evaluated using the logarithm of the minimum angle of resolution (logMAR) scale. Refractive error was reported as SE, derived by summing the spherical component and half the cylindrical component. Moreover, a mandatory criterion was the presence of at least one 6 × 6-mm radial OCT scan performed by using enhanced-depth imaging (EDI) mode, with the anterior margin of the sclera clearly visible. Both eyes were included if eligibility criteria were met. All OCT scans were reviewed by two masked expert graders (SDF and AA) and then further confirmed by a third expert grader (MBP).

The main aim of the study was to evaluate the role of DSMC in characterizing different DSM subtypes, in patients without CNV or SRD. The secondary aim was to investigate the linear relationships between the DSMC metric and CT, SE, and BCVA.

Definition of DSM and Classification

Because of the lack of an agreed-upon DSM definition and considering to the best of our knowledge the related literature,[1,10–13,18,19] we defined DSM as a convex curvature of the retinal surface, retinal pigment epithelium (RPE), and choroid, observed on OCT, protruding inward due to the underlying scleral curvature at the subfoveal level, regardless of the presence or not of posterior staphyloma. Our DSM definition aimed to provide a quantitative and standardized approach for identifying this clinical condition by including the following essential criteria:

1. The shape of the retina in a radial B-scan from OCT was mathematically modeled. Conventionally, the retinal profile is expressed by a concave function, with the curvature directed outward (Supplementary Fig. S1). In contrast, DSM is defined as a convex curvature, where the retinal surface protruded inward.[1] The point where the retinal profile transitions from concave to convex configuration, known as the inflection point, may serve as a standardized reference for evaluating DSM morphological features (Fig. 1).

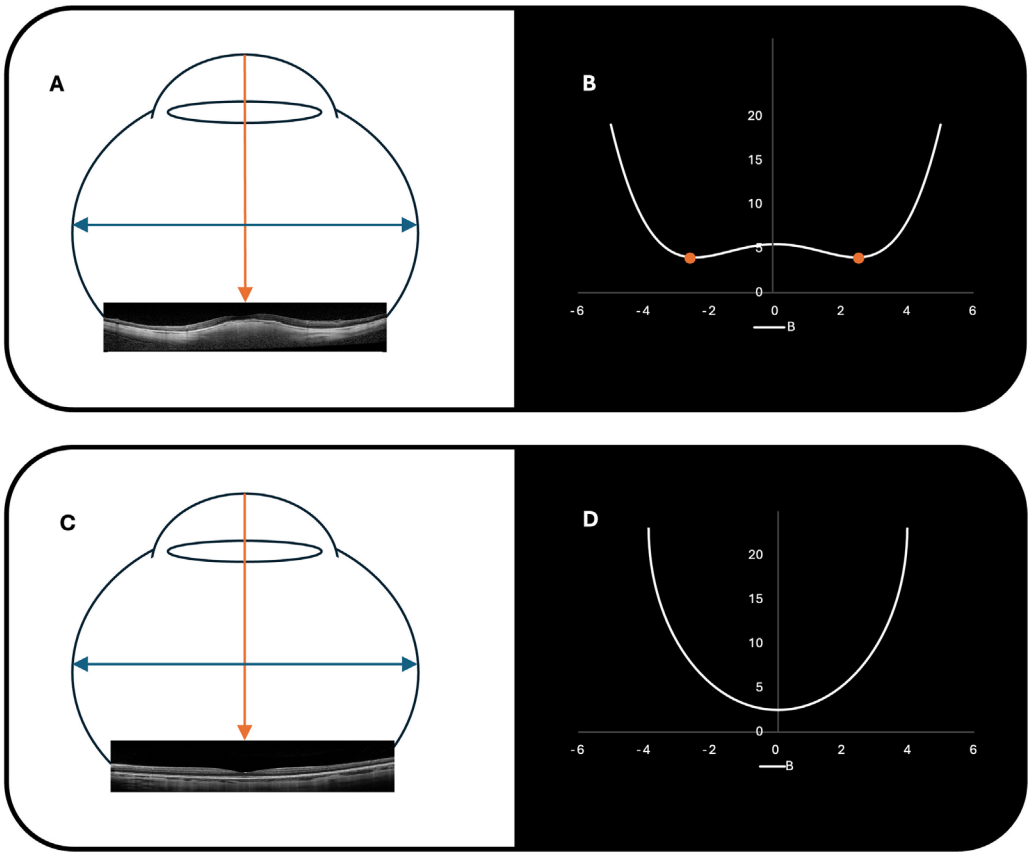

Figure 1. Two-dimensional mathematical representation of the retina. (**A**) A myopic patient with a DSM at the posterior pole. (**B**) The adjacent image illustrates how the DSM could be described using a Taylor polynomial function: $f(x) = ax^4 + bx^2 + c$, where in this specific instance $a > 0$ and $b < 0$. The *orange dots* represent the inflection points, which are points where the curve changed from concave up to concave down or vice versa. Mathematically, an inflection point occurs at the point where the function $f(x)$ changes its curvature—that is, at the point where its second derivative equals 0: $f''(x) = 0$. (**C, D**) In contrast, in a healthy patient, the posterior pole can be described by the parabolic function $f(x)=ax^2+bx+c$, where $a > 0$ and b can vary depending on the position of the vertex. Its second derivative is given by $f''(x) = 2a$, a constant value independent from x. A parabola does not have inflection points, as its curvature does not change.

2. The scleral contribution has also been considered. As suggested by Imamura et al.[2] and supported by recent evidence,[20] DSM should be considered as an anomaly of the scleral curvature. From this point of view, which differs from what has been proposed in the current literature,[1,10,12,19] the measurement of DSM morphological characteristics should also be focused on the sclerochoroidal junction.
3. DSM configuration was associated with a convex elevation located either partially or entirely below the fovea. Furthermore, current DSM definitions[1,10,12,19] commonly consider the presence of posterior staphyloma as an essential component. However, growing evidence suggests that these two entities (DSM and posterior staphyloma) may be considered two distinct conditions. To support this point, a recent study by Saito et al.[21] found that approximately 45% of DSM cases were not associated with the presence of a posterior staphyloma.
4. To validate a standardized approach, DSM should be defined based on both the curvature and the tomographic criteria. The curvature criterion may be established considering a cutoff value greater than 1 macular vertex index (Ma.V.I.), defined as 10^{-5} μm^{-1}, confirmed in at least 50% of the radial OCT scans. The presence of a Ma.V.I. < 1 may be used as exclusion criterion for DSM. The detailed description of Ma.V.I. calculation is provided in the next paragraph. In addition, Ellabban et al.[10] established that a minimum RPE elevation of 50 µm is necessary to define DSM.
5. To address potential pitfalls, and contrary to the findings by Ohsugi et al.,[19] the presence of convexity should be evaluated across all radial OCT sections and must be observed in at least 50% of these scans to address the influence

of artifacts or conditions that might mimic DSM.

In addition, our morphological classification of DSM included the categorization proposed by Caillaux et al.,[12] using both horizontal and vertical B-scans. The classification was based on the orientation of the major axis of the dome as observed on OCT: Typical round domes appeared as convex elevations in both horizontal and vertical scans, horizontally oriented domes showed marked convexity in vertical scans but were flat in horizontal scans, and, conversely, vertically oriented domes exhibited prominent convexity in horizontal scans, with flat profiles in vertical scans.

DSMC Evaluation and Image Analysis

The OCT-based calculations of DSM curvature and other parameters were conducted using 1:1-µm images. This choice was made because a previous study highlighted the potential overestimation of retinal tissue thickness when using 1:1 pixel images.[22] The measurements were carried out utilizing the Heidelberg HEYEX software and its caliper tool. Additionally, curvature was assessed in all OCT scans, with the final value corresponding to the scan showing the highest curvature.

DSM was considered a three-dimensional structure—whether dome-shaped or band-shaped—that could be approximated as a portion of a sphere or a cylinder, respectively. Our approach assumed that the DSM curvature could be derived by defining a circle traced considering DSM as a portion of the scleral curvature represented by geometric solids. When considering either a sphere or a cylinder (dome-shaped or band-shaped, respectively), a circle can be inscribed (Supplementary Fig. S2). For a sphere, any cross-section through the center produces a circle, whereas, for a cylinder, the cross-sectional circle corresponds to a plane perpendicular to the axis of the cylinder, passing through the centers of both circular bases (Fig. 2).

To measure DSMC, the distance between the inflection points on both sides of the dome was considered

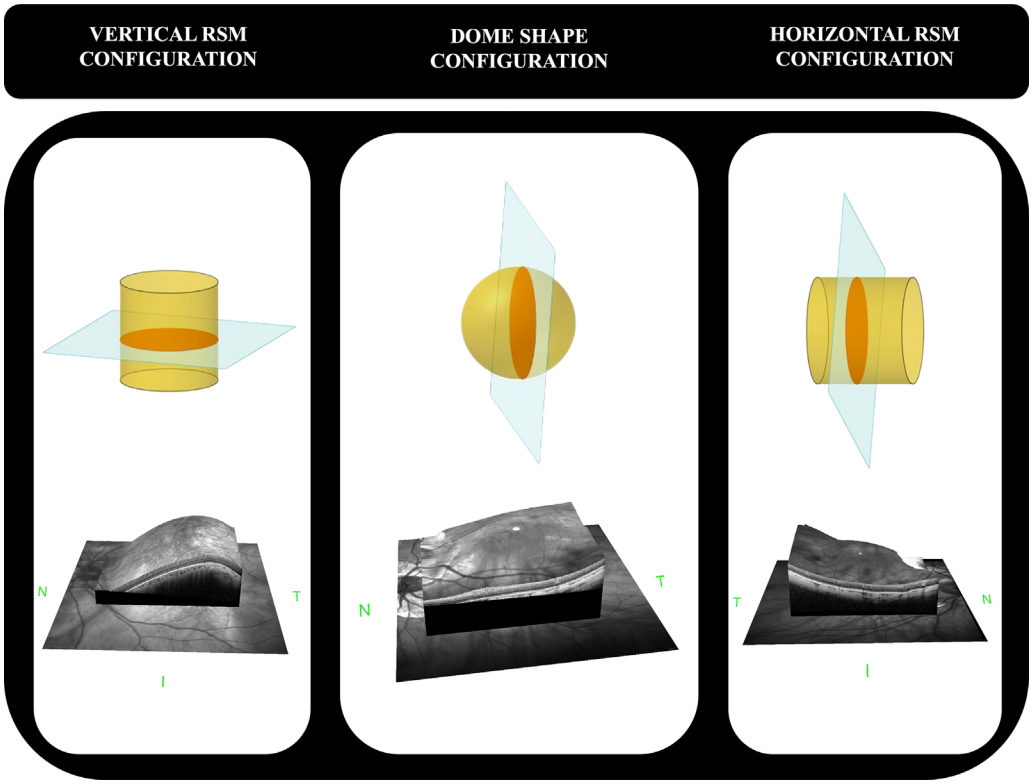

Figure 2. Schematic depiction of DSM and RSM configurations. In the center is shown the three-dimensional configuration of a round DSM. The *yellow sphere* represents the underlying geometric shape, and the dome can be thought of as the apical portion of this sphere. A *light blue plane*, passing through the center of the sphere, defines a circle, which is shown in *orange*. Similarly, the images on either side depict an RSM. On the *left*, the configuration is vertically oriented; on the right, it is horizontally oriented. In both cases, by sectioning the solid perpendicular to its major axis, a circle is obtained. The images were created with GeoGebra. Beneath each schematic are corresponding three-dimensional reconstructions of the macular profile, generated using the Heidelberg 3D Map tool. The images offer a realistic rendering of the curvature. N, nasal orientation; T, temporal orientation; I, inferior orientation.

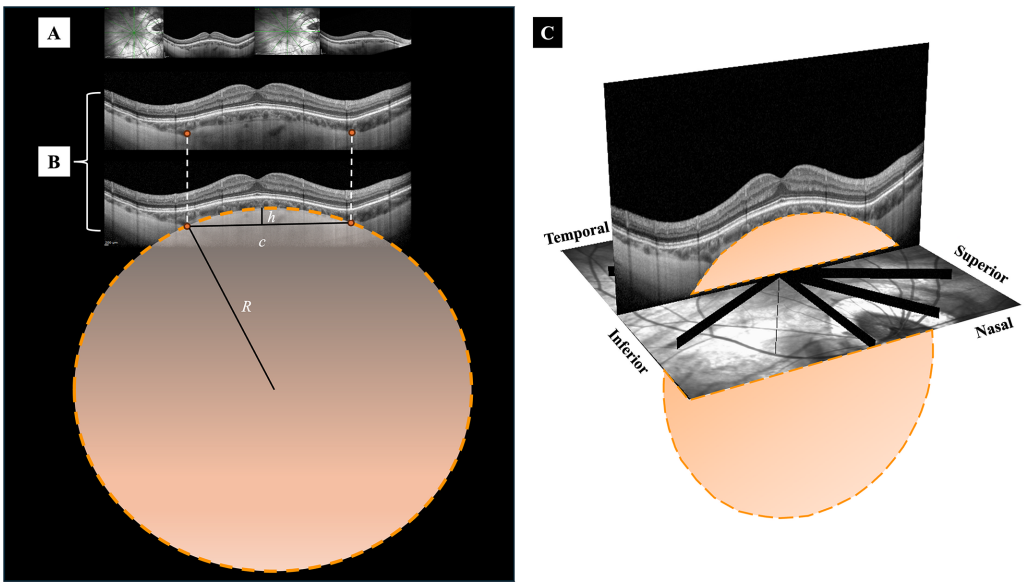

Figure 3. DSM curvature measurement. (**A**) Vertical and horizontal sections of a DSM show a horizontal RSM where the dome appeared on the vertical axis but was flat on the horizontal axis. (**B**) When the section of interest had been identified, inflection points at the sclerochoroidal junction were located. The chord (*c*) was defined as the line connecting these points, and the height (*h*) was the perpendicular line from the chord to the sclerochoroidal margin. With these measurements, the radius (*R*) of the circle was determined and is represented in *orange* beneath the dome. The curvature was then calculated as the reciprocal of this radius. (**C**) The image on the *right* was obtained using the 3D view function of the Heidelberg software. It provides a 3D description of the DSM: the floor represents the en face scan of the posterior pole, and the B-scan shows the retina in vertical section. The circle underlying the DSM is shown in *orange*. The OCT images presented were exported at 1:1-pixel resolution to enhance understanding and clarity.

(denoted as line *c* in Fig. 3). The distance from the apex of the dome, identified as the sclerochoroidal junction, to line *c* was measured as a perpendicular line (denoted as *h* in Fig. 3). We then calculated the radius (*R*) of the hypothetical circle defined by its chord *c* and height *h*. The geometric formula used to determine *R* is as follows:

$$R = \frac{h}{2} + \frac{c^2}{8h}$$

with the calculated *R*, we then determined the curvature (*K*) of the circle as the reciprocal of the radius (Fig. 3):

$$K = \frac{1}{R}$$

by definition, the curvature of a circle is constant. This means, for example, that the curvature value of an arc of the circle, such as the virtual line represented by the sclerochoroidal margin between the two inflection points, will be the same as that of any other point along its circumference. Furthermore, *K* is expressed in units of 10^{-5} μm^{-1} for consistency. For the sake of simplicity, we defined 10^{-5} μm^{-1} as 1 Ma.V.I. Hence, $K = 4 \times 10^{-5}$ μm^{-1} would be expressed as 4 Ma.V.I. All measurements were performed by the same trained ophthalmologist (AA).

Considering all of these points, DSMC may be considered a measurement that transcends the classification approach of DSM based on the configuration in OCT images. Regardless of the DSM type and considering that each of the three types (round DSM, horizontal RSM, and vertical RSM) can be approximated to a geometric structure, it is possible to evaluate the curvature in each case.

In our study, CT was manually measured at three specific locations, following the methods described by Burke et al.[23]: one at the subfoveal region and two at 3000 µm from the fovea, with the latter measurement being the average of values from both the left and right sides. Additionally, CT was measured at the inflection points of the DSM, with the final value calculated as the mean of measurements taken on either side of the DSM. All measurements were performed on horizontal EDI scans to ensure consistency across the dataset. In all cases, CT was measured perpendicularly from the outer border of the RPE–Bruch's membrane complex to the sclerochoroidal junction in the center of the fovea.

Validation of Curvature Criterion

The choice of 1 Ma.V.I. for the lower limit cut-off was based on the relationship between the curvature

and the effective R of the circle. K was the reciprocal of R, as previously shown. A curvature of 1 Ma.V.I., which equated to 10^{-5} μm^{-1}, corresponded to R equal to 10 cm. Given that the average diameter of the human eye is about 2.4 cm,[24] we assumed that a circle with a 10-cm radius would produce a nearly flat surface when compared to the curvature of the retina. Therefore, when the curvature fell below 1 Ma.V.I. (i.e., the radius exceeded 10 cm), the retinal surface became so flat that it was not consistent with the scleral curvature associated with DSM. Thus, the arbitrary selection of 1 Ma.V.I. as a threshold reflected the point at which curvature became too shallow to support a DSM diagnosis.

Considering that the resolution capability of OCT is less than 10 µm,[25] measuring curvatures for radii around this scale is challenging. Conceptually, a practical upper limit for Ma.V.I. had been set at 10,000, corresponding to a curvature of 10^{-1} μm^{-1}, which equates to a radius of 10 µm. In practical terms, an R value of 10 µm or less would not produce noticeable variations in scleral curvature, as the underlying circle would be too small. Consequently, for identifying DSM, Ma.V.I. potentially ranges from 1 to 10,000. The upper limit was established considering that greater values correspond to a radius $\leq$ 10 µm. We might assume that this value is insufficient to curve the retina enough to make a DSM. In addition, based on our cohort, values above 100 Ma.V.I. were not found. We may assume that this occurred because of OCT resolution limits and because Ma.V.I. $>$ 100 is already too insufficient to make a DSM.

Statistical Analysis

All statistical analyses were conducted using R 4.4.2 (R Foundation for Statistical Computing, Vienna, Austria). A significance level of $\alpha < 0.05$ was applied, and two-tailed tests were utilized for all comparisons. Continuous variables were described using means, standard deviations, medians, and interquartile ranges (IQRs). Categorical variables were reported as frequencies and percentages. To investigate both the differences among DSM subtypes and the associations between DSMC and ocular parameters (CT, SE, and BCVA), a consistent statistical framework was applied. A linear mixed-effects model (LMM) fit using restricted maximum likelihood (REML) was employed in both analyses. For the analysis of DSM subtypes, the model incorporated DSM subtype (round, horizontal, or vertical) as a fixed effect to evaluate subtype-specific differences, with random intercepts for patients included to address the hierarchical structure of the data and the correlation between eyes within the same patient. Similarly, to examine the associations between DSMC and CT, SE, and BCVA, the LMM was adapted to include DSMC as the fixed effect while retaining the same random structure. The use of REML ensured accurate estimation of variance components, and Satterthwaite's approximation for degrees of freedom was applied to evaluate the significance of fixed effects, providing robust and reliable estimation of P values in both analyses.

The reliability of DSMC and related measurements was assessed through interclass correlation coefficients (ICCs), calculated using a two-way random-effects model for absolute agreement. ICC values were classified as follows[26]: Less than 0.50 indicated poor reliability, 0.50 to 0.75 reflected moderate reliability, 0.75 to 0.90 indicated good reliability, and values above 0.90 represented excellent reliability. In addition, Spearman's rank correlation coefficient (r) was used to evaluate the relationships between DSMC and the other ocular parameters.

Results

This study included 125 eyes from 107 eligible patients (25 males, 23%). The mean age ± SD was 65.67 ± 13.51 years, and all patients were of Caucasian ethnicity. The DSM was unilateral in 89 patients (83%) and bilateral in 18 patients (17%). All demographic characteristics of the cohort are detailed in Table 1. With regard to the calculation of DSM height and chord length, as well as DSMC, the overall ICC was 0.95 (range, 0.89–0.97; $P < 0.05$), indicating very high intergrader reliability. The ICC for height measurements was 0.96 (range, 0.91–0.97), and the ICC for chord length measurements was 0.93 (range, 0.89–0.96).

Table 1. Demographic and Clinic Characteristics of Study Patients ($N = 107$) Affected by DSM

	Overall
Age (y)	
Mean ± SD	65.67 ± 13.51
Median (minimum, maximum)	64 (36, 95)
Male gender, *n* (%)	25 (23)
DSM status, *n* (%)	
Bilateral	18 (17)
Unilateral	89 (83)
Caucasian, *n* (%)	100 (100)

DSM, dome-shaped macula; N, number; SD, standard deviation.

Table 2. Summary of Morphological and Functional Parameters Across DSM Subtypes

Parameter	Mean ± SD			
	Overall ($n = 125$ Eyes)	Round ($n = 57$ Eyes)	Horizontal ($n = 58$ Eyes)	Vertical ($n = 10$ Eyes)
DSMC (Ma.V.I.)	20.36 ± 10.01	22.4 ± 11.4	18.3 ± 9.14	20.0 ± 4.23
Radius (µm)	6879.96 ± 5421.0	6257.0 ± 4787.0	7784.0 ± 6288.0	5182.0 ± 1003.0
Chord (µm)	3178.74 ± 1530.51	2966.0 ± 1720.0	3430.0 ± 1347.0	2935.0 ± 1276.0
Height (µm)	228.5 ± 150.82	215.0 ± 163.0	241.0 ± 134.0	236.0 ± 180.0
Subfoveal CT (µm)	65.22 ± 52.21	55.2 ± 43.3	77.2 ± 57.3	52.4 ± 57.7
CT at 3000 (µm)	82.92 ± 57.6	72.7 ± 40.4	88.8 ± 63.3	107.0 ± 92.9
CT at the inflection points (µm)	85.52 ± 65.73	75.4 ± 45.4	92.1 ± 76.0	105.00 ± 93.8
SE (D)[a]	−12.62 ± 3.62	−11.50 ± 3.80	−13.2 ± 3.34	−15.0 ± 2.68
BCVA (logMAR)[a]	0.27 ± 0.34	0.23 ± 0.29	0.29 ± 0.31	0.38 ± 0.65

BCVA, best-corrected visual acuity; CT, choroidal thickness; D, diopter; DSMC, dome-shaped macula curvature; LogMAR, logarithm of the minimum angle of resolution; Ma.V.I., macular vertex index; SE, spherical equivalent.

[a]Missing data.

Morphological and Functional Characteristics of DSM Subtypes

The distribution among the three DSM subtypes included 57 classified as round (45.6%), 58 as horizontal (46.4%), and 10 as vertical (8%), as shown in Table 2. The mean DSMC was 20.36 Ma.V.I. (SD = 10.01; IQR = 12.29–26.93). LMMs revealed that round DSM demonstrated significantly higher curvature compared to horizontal DSM (estimate = −3.884 Ma.V.I.; 95% confidence interval [CI], −7.616 to −0.152; $P = 0.039$), but vertical DSM did not differ significantly from round DSM (estimate = −2.196 Ma.V.I.; 95% CI, −9.030 to 4.638; $P = 0.527$).

The mean ± SD R (6879.96 ± 5421.0 µm), chord length (3178.74 ± 1530.51 µm), and height (228 ± 15 µm) showed no significant differences across DSM subtypes. Subtype-specific means for R were 6808 µm (round), 7761 µm (horizontal), and 5182 µm (vertical); chord length and height remained consistent across subtypes, with minimal and non-significant variations. All data are provided in Table 2.

The analysis of CT revealed no significant differences at the subfoveal level (mean, 65.22 ± 52.21 µm; $P > 0.05$). Moreover, CT measurements at 3000 µm (mean, 82.92 ± 57.60 µm) and at the inflection points (mean, 85.52 ± 65.73 µm) were consistent across subtypes without significant variations ($P > 0.05$).

Regarding refractive error and visual characteristics, BCVA was available for 117 out of 125 eyes, and SE was available for 98 out of these 117 eyes. Missing data in both cases were due to a history of cataract surgery. The mean SE for the entire cohort was −12.62 ± 3.62. Vertical DSM was significantly associated with a more pronounced myopic refractive error compared to round DSM (estimate = −3.680 D; 95% CI, −6.768 to −0.591; $P = 0.023$), and horizontal DSM showed a non-significant trend toward greater myopia (estimate = −1.200 D; 95% CI, −2.860 to 0.460; $P = 0.158$), as highlighted in Table 3. For BCVA, the mean value for the entire cohort was 0.27 ± 0.34 logMAR. Although vertical DSM showed a trend toward worse BCVA compared to round DSM (estimate = 0.144 logMAR; $P = 0.243$), this difference was not statistically significant. Horizontal DSM also did not differ significantly from round DSM (estimate = 0.063 logMAR; $P = 0.376$), as shown in Table 3.

Association Between DSMC and CT, SE, and BCVA

Analysis using LMMs highlighted significant associations between DSMC and key structural and functional parameters in DSM. Subfoveal CT exhibited a strong inverse correlation with DSMC (estimate = −0.1027; $P < 0.0001$; $r = -0.60$), with a consistent reduction in CT values as curvature increased. This inverse relationship extended to CT measured at 3000 µm from the foveal center (estimate = −0.0605; $P < 0.0001$) and at the inflection points (estimate = −0.0511; $P < 0.001$), indicating a systematic decrease in CT across all measured locations with increasing DSMC (Figs. 4A–C). DSMC was significantly associated with SE, with higher DSMC values corresponding to greater myopic refractive errors (estimate = −0.1387; $P = 0.009$; $r = -0.21$), as shown in Fig. 4D. The model also revealed variability across patients, indicating that refractive outcomes were influenced

Table 3. Mixed-Effects Model Analysis of Morphological and Functional Parameters Across DSM Subtypes

Parameter	DSM Subtype	Estimate (SE)	95% CI	P[a]
DSMC (Ma.V.I.)	Round (ref.)			
	Horizontal	−3.884 (1.866)	15.6 to 21.0	**0.039**
	Vertical	−2.196 (3.461)	13.7 to 26.3	0.527
Radius (µm)	Round (ref.)			
	Horizontal	952.91 (775.38)	6385 to 9137	0.225
	Vertical	−1625.52 (1932.73)	1612 to 8753	0.402
Chord (µm)	Round (ref.)			
	Horizontal	244.54 (235.78)	2998 to 3778	0.303
	Vertical	−208.57 (531.65)	1957 to 3912	0.696
Height (µm)	Round (ref.)			
	Horizontal	6.815 (27.197)	194 to 275	0.803
	Vertical	7.696 (52.669)	140 to 332	0.884
Subfoveal CT (µm)	Round (ref.)			
	Horizontal	20.904 (7.875)	67.1 to 93.6	0.061
	Vertical	−7.076 (18.179)	18.9 to 85.9	0.698
CT at 3000 (µm)	Round (ref.)			
	Horizontal	8.512 (10.579)	71.5 to 103.0	0.423
	Vertical	28.303 (20.498)	69.8 to 144.0	0.170
CT at the inflection points (µm)	Round (ref.)			
	Horizontal	16.102 (8.737)	79.2 to 112.0	0.072
	Vertical	25.701 (23.255)	62.0 to 148.0	0.271
SE (D)	Round (ref.)			
	Horizontal	−1.2005 (0.8415)	−13.8 to −11.25	0.158
	Vertical	−3.6799 (1.5747)	−17.9 to −12.14	**0.023**
BCVA (logMAR)	Round (ref.)			
	Horizontal	0.06258 (0.07044)	0.20 to 0.397	0.376
	Vertical	0.14411 (0.12270)	0.16 to 0.600	0.243

Dependent variables are the parameters of interest (DSMC, radius, chord, height, CT, SE, BCVA).
[a]Statistically significant *P* values are bold.

by additional, unmeasured factors, contributing to interindividual differences. In contrast, for BCVA, DSMC showed no significant correlation (estimate = 0.0054; $P = 0.082$) (Fig. 4E).

Discussion

This study proposed a comprehensive analysis of the morphological and functional parameters of DSM, particularly focusing on DSMC as a new quantitative metric. To the best of our knowledge, this is the largest study assessing the morphological parameters of a cohort of DSM without complications such as CNV and SRD. DSMC provides an objective and repeatable measure to categorize DSM and offers new insights into DSM morphology.

In terms of prevalence, vertical DSM subtypes resulted an uncommon finding, as previously reported in the literature. In the large cohort study by Liang et al.,[5] vertical subtypes accounted for only 2% of cases, with five instances identified out of 225 eyes. As already reported in the literature,[10,12] round and horizontal subtypes were more common, with horizontal forms showing a slight predominance.

Looking at the geometric characteristics of DSM, our results revealed a significant difference in curvature between round and horizontal DSM subtypes, but no significant difference was observed between round and vertical DSM subtypes. This finding may seem unexpected at first, as differences in chord length and height are present among the three groups, but they did not reach statistical significance. However, this can be explained by the quadratic relationship between chord length and curvature: Small variations in chord length can have a much greater effect on curvature compared to height.

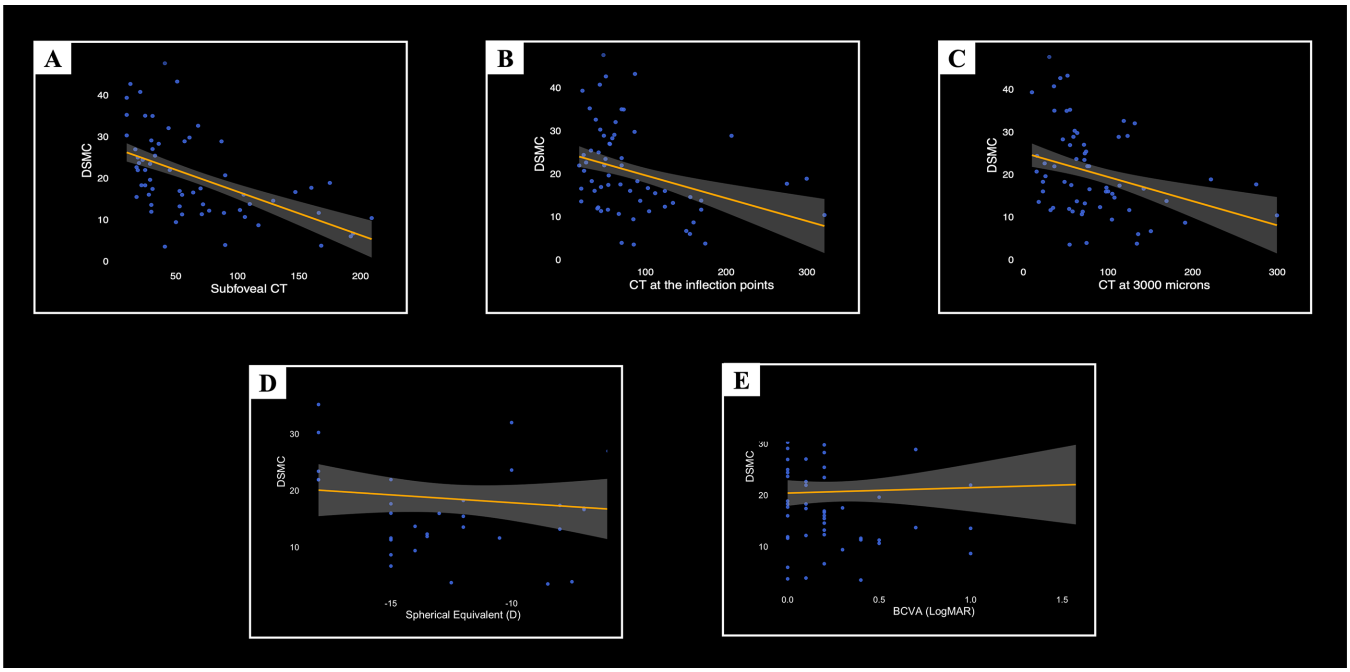

Figure 4. LMM analyses examining the relationships between DSMC and key structural and functional parameters in DSM. (**A**–**C**) Significant inverse relationships between DSMC and CT values at the subfoveal level, the inflection points, and 3000 µm from the fovea, respectively. (**D, E**) Associations of DSMC with SE and BCVA, the latter expressed in logMAR values.

We confirmed some DSM features already described in the literature.[13,28–30] Indeed, based on our observations, round DSM subtypes are morphologically characterized by smaller base and height dimensions compared to horizontal DSM subtypes, which therefore appear larger. On the other hand, vertical subtypes exhibited a slightly greater height on average compared to round subtypes.

A big part of our analysis was focused on testing the distribution of CT, BCVA, and SE considering the DSM Caillaux classification.[12] No significant differences in CT values were observed across the three DSM subtypes (round, horizontal, and vertical) at any of the measured locations: subfoveal, at the inflection points, or 3000 µm from the fovea. Previous studies by Pilotto et al.[30] and Negrier et al.[31] suggested that vertical DSMs tend to have a higher bulge and thicker CT, whereas Zhao et al.[32] reported greater CT thickness in round domes. These discrepancies may be partially attributed to differences in study designs and included populations. Indeed, prior investigations did not account for the presence or absence of CNV or SRD in their cohorts. Because it is well established that CNV in DSM is associated with partially preserved CT[33] and SRD with thicker choroids,[12] the inclusion of these patients in previous studies may have introduced a potential confounding factor. In our study, we considered only cases without CNV or SRD, providing a quantitative assessment focused on this specific "uncomplicated" DSM phenotype. Overall considering our findings, we confirmed previous observations highlighting the intrinsic limitations of Caillaux classification to fully categorize DSM clinical characteristics.[31]

Trying to overcome this issue, we evaluated the relationship between the newly introduced DSMC metric and other ocular parameters. Our results showed an inverse relationship between DSMC and CT across all measured locations, with higher curvature values corresponding to reduced CT. This indicates that DSM cases with larger base and height dimensions tend to exhibit greater CT, and vice versa. On this basis, we may hypothesize that scleral curvature in DSM influences the underlying choroidal tissue, leading to pronounced thinning, particularly in the subfoveal region. The significant relationship between DSMC and CT is potentially clinically relevant, as it may represent a measure of choroidal trophism, paving the basis for new outcome measures and risk stratification assessment in high myopia.

DSMC also demonstrated an association with SE, highlighting a link between increased curvature and higher myopic refractive errors. Based on the current design of the study and the intrinsic limitations of OCT imaging, we are not able to provide a definite explanation of this finding. We might hypothesize that DSMC

represents a surrogate measurement of the biomechanical effects of axial length on the magnitude of DSM curvature. We cannot exclude a secondary hypothesis related to a direct scleral contribution on the determination of DSM curvature extent. However, further studies with histology support are warranted to draw definite conclusions regarding this point. Conversely, no significant association was observed for DSMC and BCVA. This was expected, as visual acuity has been evaluated accounting for the refractive error of the eye.

Our study has several potential limitations. First, the retrospective and cross-sectional design may impose constraints on our analysis. The lack of longitudinal follow-up limits our ability to observe dynamic changes in DSM over time and to establish causative relationships. Additionally, further investigations should explore the association between DSMC and other potential contributing factors, such as axial length and scleral thickness, which may enhance our understanding of DSM pathophysiology and its functional consequences. Moreover, although we represented DSM as circles for simplicity, it was important to acknowledge that DSM did not conform perfectly to geometric shapes, a consideration that may have introduced relevant approximations. In addition, imaging in highly myopic eyes also presented significant challenges due to extreme curvature changes, which increased the risk of artifacts and measurement inaccuracies.[34] Moreover, the intrinsically limited depth of OCT technology does not allow addressing the scleral contribution to DSM development. Another limitation is the use of a single spectral-domain OCT device, which restricts the generalizability of our findings. Future studies should assess the reproducibility of DSMC using different imaging platforms to validate the robustness of this metric across devices.

Furthermore, the study sample was composed exclusively of Caucasian patients, with limited variability in age. Expanding the cohort to include a more ethnically and demographically diverse population would improve the generalizability and allow for a better understanding of DSM across different patient groups. Further studies and histologic confirmation are necessary to support our hypotheses and to assess the relevance of our proposed approach on the management of this condition and future therapeutic strategies.

In conclusion, we proposed a novel quantitative metric to analyze and categorize DSM subtypes. Our study indicated that the proposed DSMC metric could serve as an objective and repeatable way to categorize DSM. The significant association between DSMC and CT also suggested that DSMC could serve as a future outcome measure for monitoring CT in DSM. Further studies are warranted to test the clinical role of DSMC and its relevance in improving DSM diagnostic and therapeutic workups.

Acknowledgments

The authors thank Piero Mazzolini for his assistance with this study.

Disclosure: **S. Del Fabbro**, None; **A. Arrigo**, None; **L. Bianco**, None; **A. Antropoli**, None; **A. Nunziata**, None; **U. Introini**, None; **D. Giusto**, None; **F. Bandello**, AbbVie (C), Alimera Sciences (C), Bayer Schering Pharma (C), Boehringer Ingelheim (C), Breye Therapeutics (C), Fidia Sooft (C), Hoffmann-La Roche (C), Novartis (C), NTC Pharma (C), Outlook Therapeutics (C), Oxurion (C), SIFI (C); **M. Battaglia Parodi**, None

References

1. Gaucher D, Erginay A, Lecleire-Collet A, et al. Dome-shaped macula in eyes with myopic posterior staphyloma. *Am J Ophthalmol*. 2008;145(5):909–914.e1.
2. Imamura Y, Iida T, Maruko I, Zweifel SA, Spaide RF. Enhanced depth imaging optical coherence tomography of the sclera in dome-shaped macula. *Am J Ophthalmol*. 2011;151(2):297–302.
3. Shin E, Park KA, Oh SY. Dome-shaped macula in children and adolescents. *PLoS One*. 2020;15(1):e0227292.
4. Ceklic L, Wolf-Schnurrbusch U, Gekkieva M, Wolf S. Visual acuity outcome in RADIANCE study patients with dome-shaped macular features. *Ophthalmology*. 2014;121(11):2288–2289.
5. Liang IC, Shimada N, Tanaka Y, et al. Comparison of clinical features in highly myopic eyes with and without a dome-shaped macula. *Ophthalmology*. 2015;122(8):1591–1600.
6. Errera MH, Michaelides M, Keane PA, et al. The extended clinical phenotype of dome-shaped macula. *Graefes Arch Clin Exp Ophthalmol*. 2014;252(3):499–508.
7. Dormegny L, Liu X, Philippakis E, et al. Evolution of dome-shaped macula is due to differential elongation of the eye predominant in the peri-dome region. *Am J Ophthalmol*. 2021;224:18–29.
8. Zhao X, Ding X, Lyu C, et al. Observational study of clinical characteristics of dome-shaped

macula in Chinese Han with high myopia at Zhongshan Ophthalmic Centre. *BMJ Open*. 2018;8(12):e021887.
9. Hocaoglu M, Ersoz MG, Sayman Muslubas I, Arf S, Karacorlu M. Factors associated with macular complications in highly myopic eyes with dome-shaped macular configuration. *Graefes Arch Clin Exp Ophthalmol*. 2019;257(11):2357–2365.
10. Ellabban AA, Tsujikawa A, Matsumoto A, et al. Three-dimensional tomographic features of dome-shaped macula by swept-source optical coherence tomography. *Am J Ophthalmol*. 2013;155(2):320–328.e2.
11. Xu X, Fang Y, Jonas JB, et al. Ridge-shaped macula in young myopic patients and its differentiation from typical dome-shaped macula in elderly myopic patients. *Retina*. 2020;40(2):225–232.
12. Caillaux V, Gaucher D, Gualino V, Massin P, Tadayoni R, Gaudric A. Morphologic characterization of dome-shaped macula in myopic eyes with serous macular detachment. *Am J Ophthalmol*. 2013;156(5):958–967.e1.
13. García-Zamora M, Flores-Moreno I, Ruiz-Medrano J, et al. Dome-shaped macula versus ridge-shaped macula eyes in high myopia based on the 12-line radial optical coherence tomography scan pattern. Differences in clinical features. *Diagnostics*. 2021;11(10):1864.
14. Flitcroft DI, He M, Jonas JB, et al. IMI–Defining and classifying myopia: a proposed set of standards for clinical and epidemiologic studies. *Invest Ophthalmol Vis Sci*. 2019;60(3):M20.
15. Ohno-Matsui K, Kawasaki R, Jonas JB, et al. International photographic classification and grading system for myopic maculopathy. *Am J Ophthalmol*. 2015;159(5):877–883.e7.
16. Hubschman JP, Govetto A, Spaide RF, et al. Optical coherence tomography-based consensus definition for lamellar macular hole. *Br J Ophthalmol*. 2020;104(12):1741–1747.
17. Duker JS, Kaiser PK, Binder S, et al. The International Vitreomacular Traction Study Group classification of vitreomacular adhesion, traction, and macular hole. *Ophthalmology*. 2013;120(12):2611–2619.
18. Fang Y, Jonas JB, Yokoi T, Cao K, Shinohara K, Ohno-Matsui K. Macular Bruch's membrane defect and dome-shaped macula in high myopia. *PLoS One*. 2017;12(6):e0178998.
19. Ohsugi H, Ikuno Y, Oshima K, Yamauchi T, Tabuchi H. Morphologic characteristics of macular complications of a dome-shaped macula determined by swept-source optical coherence tomography. *Am J Ophthalmol*. 2014;158(1):162–170.e1.
20. Ohno-Matsui K, Igarashi-Yokoi T, Azuma T, et al. Polarization-sensitive OCT imaging of scleral abnormalities in eyes with high myopia and dome-shaped macula. *JAMA Ophthalmol*. 2024;142(4):310.
21. Saito R, Shinohara K, Tanaka N, Takahashi H, Yoshida T, Ohno-Matsui K. Association between dome-shaped macula and posterior staphyloma in highly myopic eyes investigated by ultra-widefield optical coherence tomography. *Retina*. 2021;41(3):646–652.
22. Kim JH, Kang SW, Ha HS, Kim SJ, Kim JR. Overestimation of subfoveal choroidal thickness by measurement based on horizontally compressed optical coherence tomography images. *Graefes Arch Clin Exp Ophthalmol*. 2013;251(4):1091–1096.
23. Burke TR, Wu AD, Shen Y, Rajendram R. Longitudinal follow-up of dome-shaped macula. *Eye*. 2020;34(10):1903–1908.
24. Bekerman I, Gottlieb P, Vaiman M. Variations in eyeball diameters of the healthy adults. *J Ophthalmol*. 2014;2014:1–5.
25. Singh SR, Chhablani J. Optical coherence tomography imaging: advances in ophthalmology. *J Clin Med*. 2022;11(10):2858.
26. Koo TK, Li MY. A guideline of selecting and reporting intraclass correlation coefficients for reliability research. *J Chiropr Med*. 2016;15(2):155–163.
27. Metz CE. Basic principles of ROC analysis. *Semin Nucl Med*. 1978;8(4):283–298.
28. Hsu CR, Igarashi-Yokoi T, Liang IC, Ohno-Matsui K. Ten-year longitudinal morphological changes in dome-shaped maculas in highly myopic eyes. *Retina*. 2023;43(11):1852–1862.
29. García-Ben A, Sanchez MJM, Gómez AG, García-Basterra I, García AS, García-Campos JM. Factors associated with serous retinal detachment in highly myopic eyes with vertical oval-shaped dome. *Retina*. 2019;39(3):587–593.
30. Pilotto E, Guidolin F, Parravano M, et al. Morphofunctional evaluation in dome-shaped macula. *Retina*. 2018;38(5):922–930.
31. Negrier P, Couturier A, Gaucher D, et al. Choroidal thickness and vessel pattern in myopic eyes with dome-shaped macula. *Br J Ophthalmol*. 2022;106(12):1730–1735.
32. Zhao X, Lian P, Li S, Liu B, Ding X, Lu L. Patterns of choroidal deepening in highly myopic

eyes with dome-shaped macula. *Curr Eye Res*. 2020;45(8):1017–1023.
33. Arrigo A, Aragona E, Bianco L, et al. The clinical role of the choroidal assessment in high myopia: characteristics and association with neovascular and atrophic complications. *Invest Ophthalmol Vis Sci*. 2023;64(12):16.
34. Arrigo A, Aragona E, Battaglia Parodi M, Bandello F. Quantitative approaches in multimodal fundus imaging: state of the art and future perspectives. *Prog Retin Eye Res*. 2023;92:101111.